Fretting corrosion damage of total hip prosthesis: Friction coefficient and damage rate constant approach

Kyungmok Kim, Jean Geringer, Julie Pellier, Digby D. Macdonald

Fretting Corrosion Damage of Total Hip Prosthesis: Friction Coefficient and Damage Rate Constant Approach

Kyungmok Kim[1], Jean Geringer[2,3*], Julie Pellier[2], Digby D. Macdonald[3,4]

[1]School of Aerospace and Mechanical Engineering, Korea Aerospace University,
100 Hanggongdae gil, Hwajeon-dong, Deogyang-gu, Goyang, Gyeonggi-do,
412-791, Republic of Korea
[2]Ecole Nationale Supérieure des Mines de Saint-Etienne,
CIS-EMSE, CNRS :UMR5146, LCG, F-42023 Saint-Etienne France
[3]Penn State University, MSE-CEST, 206A-201 Steidle Building,
University Park 16802 PA USA
[4]Chair Professor
Center for Research Excellence in Corrosion
Research Institute
King Fahd University of Petroleum and Minerals
Dhahran, Saudi Arabia

***** corresponding author.

Abstract

This paper analyzes friction coefficient evolution between materials related to total hip prosthesis. Fretting corrosion tests were conducted with stainless steel and poly (methyl methacrylate) interacting surfaces. In the course of fretting corrosion tests, the Coulomb friction coefficient is determined as a function of the number of cycles. It was found that the friction coefficient growth rate can be expressed as a power-law function. The influences of ionic strength, applied potential, pH, and albumin content on fretting corrosion were then investigated on the basis of the evolution of the friction coefficient. Finally, we identify the damage rate constant as being relevant for linking the mechanical and chemical parameters in the evolution of damage.

Keywords: Fretting corrosion; Microslip, Ionic strength, Damage Rate Constant.

1. Introduction

Fretting corrosion is known as a contact degradation phenomenon in an aqueous environment [1,2] Fretting corrosion is one of the most critical issues in the design of total hip prostheses, since it occurs at the contact surface between femoral stem and bone cement [1,2]. Fretting in a total hip prosthesis, results from destruction of the passive oxide layer on the metal, thereby leading to enhanced corrosion, and to the generation of debris, such as polymer particles [3-5] and/or metallic oxides [6], which lead to serious malfunctioning of hip joint. Cyclical loading, due to daily human gait, and differences in the mechanical properties between the femoral stem and the bone cement, give rise to disbonding between two materials. Such disbonding results in side effects, such as cement degradation and cracking. Debris, including metal oxides and ions, invade bone tissues via cracks and eventually induce the inflammation in the bone tissues [7]. Currently, cobalt-chromium

* Corresponding author. E-mail: geringer@emse.fr, jag54@psu.edu Tel: +33 477 426 688, Fax: +33 477 420 157

alloys, titanium alloys, or austenitic stainless steels are used for the fabricating femoral stems. Austenitic stainless steels (e.g., Type 316L SS) maintain good biocompatibility and high resistance against corrosion. Bone cement, such as poly (methyl methacrylate), is inserted into cancellous and cortical bones. Fretting corrosion damage between 316L SS and poly (methyl methacrylate) was experimentally investigated under the condition similar to those found at the interface between a femoral stem and bone cement [8,9] in an actual prosthesis. Dissipated interfacial energy and wear volume were measured after 2000 cycles [8]. It was demonstrated that wear volume can be expressed as a function of the interfacial energy dissipated. Meanwhile, fretting corrosion tests were interrupted after 80000 cycles [9]. Fretting phenomena in both air and in aerated solutions were studied. In air exposure, no significant wear was observed on the stainless steel, whereas mechanical wear was found when in contact with PMMA. It was found that the wear volume on PMMA is linearly correlated with the accumulated, dissipated energy.

The level of fretting damage is determined by the relative slip amplitude between the femoral stem and the bone cement. If the slip amplitude is so small that some parts at contact remain adhered and others slip over the other mating surface, cracks are dominantly generated near the contact edges (fretting fatigue). If the slip amplitude is sufficiently high to make all parts on one surface slip over the other surface, wear (loss of material) occurs over the entire contact surface (fretting wear). It was identified by numerical modelling that the slip amplitude is approximately 0.05 mm between the femoral stem and bone cement under applied stresses during normal human gait [10]. In addition, it was observed that the slip amplitude induces fretting wear in total hip prostheses [11]. The chloride concentration (ionic strength), protein (albumin) concentration, and pH of the solution could affect fretting (corrosion) damage of materials involved in a total hip prosthesis. The influences of ionic strength, albumin, and applied potential were studied in the authors' earlier paper [11]. Fretting corrosion tests were conducted using 316L SS and PMMA. After interrupting the fretting tests, the worn surfaces were profiled and wear volumes were measured. It was determined that the ionic strength increases the wear volume on 316L SS at the open circuit potential. Albumin of 1 g L^{-1} does not play a significant role in determining the 316L SS total wear volume, in comparison with 0 g. L^{-1} of albumin. At an applied potential of E = −0.4 V(SCE), a threshold concentration of 0.1 M (NaCl solution) exists above which metal dissolution becomes enhanced. Finally, albumin of 20 g.L^{-1} decreases the wear volume of the 316L SS, but it increases the wear volume of the PMMA.

For the purpose of evaluating fretting performance of a material, the friction coefficient can be used as a practical metric. During fretting tests, the tangential force and the relative displacement at the contact are typically measured. Thus, the Coulomb friction coefficient, the ratio of tangential force to the normal force, can be calculated. That is, it is possible to monitor friction behaviour at a contact surface without interrupting a fretting test. For this reason, the friction coefficient, as well as wear volume (post mortem measurement), has been widely used for investigating tribological properties of coated or non-coated systems [12,13]. In addition, from the experimental data, including tangential force and relative displacement, a force-displacement plot can be drawn, called a "fretting loop". A fretting loop is informative, since it can show the transition between the partial slip regime and the gross slip regime. The area within the fretting loop corresponds to the energy dissipated by the contacting surfaces. The ratio of the dissipated energy to the total energy is used for identifying the transition between the wear-dominant regime and the fatigue-dominated regime [14]. If the ratio remains below 0.2 during a fretting test, it was determined that the test was performed under the fatigue-dominated regime. Otherwise, the test was identified as being conducted within the wear-dominated regime. For this reason, it is necessary to monitor the ratio when investigating fretting wear.

Earlier research [11] did not include investigation of the friction behaviour. Characterization of the evolution of the friction coefficient is useful for understanding friction behaviour of uncoated systems and for predicting the durability of coated systems. If the evolution of the friction

coefficient can be described by an appropriate mathematical function, it can be possible to quantify the influences of the experimental parameters (chemical properties, such as ionic strength, albumin concentration, pH, etc) on the friction coefficient evolution. The ultimate goal is to link the chemical parameters of the system to the tribological parameters, such as friction coefficient and the energy ratio.

A variety of studies of friction in total hip prostheses have been performed [15-19]. The friction behaviour of polymer/polymer hydrogels for articular cartilage was investigated with a pin-on-disk apparatus [15]. Polymer content of poly (vinyl alcohol)/poly (vinyl pyrrolidone) hydrogels, load, and influence of lubricant were studied. Tribological properties of stainless steels for the hip material were investigated in several lubricants (Hanks' balanced salt solution, and solutions of bovine serum albumin and of hyaluronic acid) [16]. The friction coefficient between Ti-6Al-4V and PMMA was determined by the standard, inclined plane test [17]. Friction testing was conducted under dry and wet conditions; the latter using Ringer's solution and bovine serum. The static coefficient of friction between stainless steel and PMMA used in cemented hip and knee implants were determined [184]. Sliding friction tests were conducted under dry and wet conditions using bovine serum. The influence of surface roughness and contact pressure on the friction coefficient was investigated. Wear of poly (methyl methacrylate) against stainless steel was investigated under dry conditions [19]. The relationship between wear volume and accumulated, dissipated energy was studied.

In this study, friction behaviour between stainless steel and PMMA was investigated under wet conditions. The evolution of the Coulomb friction coefficient was measured and expressed as an appropriate mathematical function. The influence of ionic strength, albumin, applied potential, and pH of the solution on the evolution of the friction coefficient was thereby investigated.

2. Experimental setup

One parallelepiped specimen (9 mm x 9 mm x 20 mm) and one cylindrical pad (a length of 15 mm and a radius of 10 mm) were used for each fretting corrosion test. The specimen for femoral stem was made of stainless steel (316L). The contact surface of the specimen was polished with diamond paste down to 1 µm prior to a test. Initial surface roughness was measured as being approximately 10 ± 2 nm over an area of 2 mm^2 by using Veeco™ optical profilometry. The cylindrical pad corresponding to bone cement was made of poly (methyl methacrylate) (PMMA). The mechanical properties of the polymer are similar to those of bone cement; mechanical properties of PMMA supplied by the manufacturer were elastic modulus of 2.5 GPa, Poisson's ratio of 0.39, yield strength of 65 MPa, and tensile strength of 75 MPa. The contact surface of the pad was polished with 3 µm diamond solution (Altuglass® Polish 1 and 2) and a colloidal solution of silica. The initial surface roughness was about 35 ± 5 nm. All specimens and pads were stored in a desiccator for 24 hours prior to an experiment. During the tests, the 316L SS specimens were electrically insulated from the fretting corrosion device with oxidized Zircalloy sheets and electrical varnish.

Fretting corrosion tests were performed at room temperature and in NaCl solutions of 0.001, 0.01, 0.1, 0.155, and 1 M. For investigating the influence of protein, albumin of 1 $g.L^{-1}$ or 20 $g.L^{-1}$ was added in separate solutions.

[Fig. 1]

Figure 1 shows the fretting corrosion testing machine [11]. An electromagnetic motor located on the left side was used for producing fretting under contact loading. A load transducer for measuring tangential force at contact was placed on the right side. A capacitive sensor measured the relative displacement between the specimen and the pad. One might suggest that inertial forces

play a significant role in this kind of device. As shown in Figure 1, a specific bumper was inserted between the motor and the sample holder. The load transducer is fixed at the end of the arm, as shown in Figure 1. The bumper was inserted for controlling the motor response to the change of sliding direction during the fretting corrosion experiments. Indeed, the mechanical response of the device, without the bumper, was too quick and the system is too sensitive to stick-slip phenomena, for example. The inertial forces are included in the compliance analysis shown in Ref. [11]. The most important point was controlling the compliance of the device, during each test and amongst all tests, in order to be sure that it is constant. Thus, the actual displacement is a little different than the imposed one, as shown in Ref. [11]. For reproducing fretting between the specimen and the pad, a normal force of 127.5 N (a pressure of approximately 22 MPa) was applied, and a displacement amplitude of ± 0.04 mm close to the *in vivo* displacement was induced using a sinusoidal waveform [11]. A frequency of 1 Hz was applied, assuming that the frequency was similar to the human gait cycle per second. During a test, a tangential force and a relative displacement were recorded and the Coulomb friction coefficient was determined.

3. Results and discussion

Fretting corrosion tests were performed by changing the ionic strength, albumin content, and pH. The open circuit potential (OCP) was measured between the working electrode, 316L SS, and a reference electrode, SCE [Standard Calomel Electrode, +246 mV vs. the Standard Hydrogen Electrode (SHE)] in a three-electrode configuration, with the third electrode being the current-carrying counter electrode. Additionally, a potential of –400 mV was applied between the working electrode and the reference electrode, SCE, using a Potentiostat, PARSTAT 2263, which also measures the current flowing between the working electrode and the counter electrode. In this study, the evolution of the friction coefficient was measured during fretting cycles and analyzed. Fretting loops were monitored, and dissipated energy and total energy in each fretting loop were computed.

3.1 Influence of ionic strength

For the purpose of investigating the influence of ionic strength on the evolution of the friction coefficient, five ionic strengths were selected, as shown in Figure 2. Fretting tests were interrupted after 14,280 cycles; sufficient duration for highlighting the dependence of the friction coefficient on the chemical parameters.

[Fig. 2]

Figure 2 shows the evolution of the friction coefficient at five ionic strengths: 0.001, 0.01, 0.1, 0.155 and 1 M. The evolution of the friction coefficients can be divided into three distinct stages. In the primary stage, the friction coefficient value rapidly dropped. For instance, at an ionic strength of 0.01 M, the initial friction coefficient was 0.61. The value decreased to 0.46 after 360 cycles. The friction coefficient values at ionic strengths of 0.01, 0.1 and 1 M also declined. Meanwhile, the evolution of the friction coefficient at ionic strengths of 0.001 and 0.155 M did not show an initial decrease of the friction coefficient. A possible reason might be related to the initial surface roughness. Partial solid asperity contact might exist in the cases of 0.01, 0.1 and 1 M ionic strengths. A solid asperity contact zone was then reduced in size and roughness with increasing number of cycles. When the solid asperity contact zone was minimised and fluid film lubrication was maximised at the contact (approximately 500 cycles), the friction coefficient evolved to be low. Meanwhile, in the cases of 0.001 and 0.155 M, initial solid asperity contact zones were relatively small. Specially, at 0.001 M, the initial contact might be subjected to almost full-fluid film lubrication. For this reason, the initial friction coefficient seemed to be relatively low.

In the secondary stage, the friction coefficient rapidly increased in all cases; surface roughness should increase and it is postulated that the solid asperity contact zone between 316L and PMMA could come to be larger. Finally, the solid asperity contact came to prevail over the entire contact, and the friction coefficient remained high (tertiary stage).

[Fig. 3]

After each fretting cycle, a quasi-rectangular fretting loop was observed. The area within the fretting loop is equal to dissipated energy (E_d). The ratio of the dissipated energy to the total energy can be used for classifying slip regimes (fatigue-dominated or wear-dominated), as noted earlier in this paper. The ratio of the dissipated energy to the total energy was defined as the energy ratio [10]

$$Energy\,ratio = \frac{E_d}{E_t} \quad (1)$$

where E_t is total energy and is computed as $4 \times Q_{max} \times \delta_{max}$. Q_{max} is a maximum tangential force and δ_{max} is a maximum displacement in a fretting loop. If the *energy ratio* remains above 0.2 during a test, it was suggested that a fretting test is conducted within the (mechanical) wear-dominated regime. Figure 3 shows the evolution of the energy ratio for different ionic strengths. All values of the energy ratio remain above 0.2, indicating that fretting tests were finished within the (mechanical) wear-dominated regime. Up to 500 cycles, the energy ratio increased rapidly. After starting a test, partial asperity contact between samples might exist. During the first 500 cycles, fretting is deemed to reduce the size of the asperities and hence the friction at the contact surfaces. Reduced asperity allows for a larger sliding distance at the contact surfaces, eventually leading to the increase of the dissipated energy within a fretting loop.

In order to understand friction behaviour in the secondary stage, the measured evolution of the friction coefficient needs to be described by an appropriate mathematical function. In this study, it was found that the friction coefficient growth rate in the secondary stage can be expressed as a power-law function of the number of cycles. That is, the relation between friction coefficient growth rate (*df/dN*) and number of cycles (*N*) is

$$\frac{df}{dN} = C \times N^m \quad (2)$$

where *C* is the damage rate constant and *m* is the damage exponent. If *m* is close to -1, the friction coefficient may be expressed as

$$f = f_0 + C \times \ln(\frac{N}{N_0}) \quad (3)$$

where f_0 is initial friction coefficient and N_0 is the number of cycles at the beginning of the secondary stage. Appendix B shows the cycle number at the beginning of the secondary stage. The number of cycles, when the secondary stage starts, clearly depends upon the experimental conditions.

[Fig. 4]

For determining the parameters in Equation 2, experimental data (within the range from a few hundred to 5000 cycles, depending on the specific evolution) were fitted with a power-law function, as shown in Appendix A. Then, the derivative of the friction coefficient evolution was calculated. The damage rate constant (*C*) and the damage exponent (*m*) can be determined from the *df/dN* versus *N* plots on the bilogarithmic scale, as shown in Fig. 4. The damage exponent is close to -1. The actual synovial fluids are more complicated than those considered in this experiment. This could be the reason why the damage rate exponents were not equal to -1. Meanwhile, the damage rate constants are dependent upon the ionic strength.

[Fig. 5]

Figure 5 shows the relationship between the damage rate constant and ionic strength. Between 0.001 and 0.1 M in ionic strength, the damage rate constant values are similar. In the case

that the ionic strength is greater than 0.1 M, the damage rate constant value significantly decreases as the ionic strength increases. That is, an ionic strength lower than 0.1 M does not greatly affect the evolution of the friction coefficient in the secondary stage. Figure 5 is meaningful and fruitful, because it allows highlighting the breakdown ionic strength (corresponding to the change in slope of *C* vs ionic strength) of 0.1 M. This phenomenon was described in Ref. [7]; below 0.1 M, damage accumulation is related to mechanical wear, but above this value of the ionic strength, damage is associated with corrosive wear (fretting corrosion).

3.2 Influence of applied potential

In order to the evaluate the friction coefficient between femoral 316L SS and PMMA at the applied potential of -0.4 V/SCE, a fretting corrosion test was conducted at zero albumin and at an ionic strength of 1 M.

[Fig. 6]

Figure 6 shows the differences in the friction coefficient evolutions measured at the OCP and at -0.4V/SCE. Differently from the evolution of the friction coefficient at the OCP, the initial friction coefficient value at -0.4 V/SCE was high. The friction coefficient tends to increase up to 0.57 (until 7500 cycles), followed by a decrease to 0.51. During a fretting corrosion test, the potential was recorded under open circuit conditions. The initial potential was determined to be -0.3 V/SCE and then it decreased sharply. The OCP gradually decreased after the initial rapid drop. One might suggest that this evolution is as expected under tribocorrosion experimental conditions.

[Fig. 7]

Figure 7 shows the relationship between the friction coefficient and the open circuit potential (OCP) for cycle numbers up to 5000. It is observed that the friction coefficient presents an inverse linear relationship with potential. For cycle numbers greater than 5000, the friction coefficient and the potential gradually decreased together. This graph is useful for displaying the linear relationship and presents the effective format for the comparing results.

[Fig. 8]

Figure 8 shows the evolution of the energy ratio at the OCP and at -0.4 V/SCE. All of the energy ratios at -0.4 V/SCE were greater than 0.6 and were higher than those for the OCP. It was concluded from the plot that the fretting corrosion test at -0.4 V/SCE was completed within the wear-dominated regime due to higher energy ratio; i.e., little fretting corrosion occurred.

3.3 Influence of albumin

Fretting corrosion tests were conducted with a saline solution including various albumin contents for the purpose of understanding the role of proteins. In this study, two different contents of albumin were added to the solution. Other experimental conditions are that the experiments were conducted at the OCP and at an ionic strength of 0.001 M. The friction coefficient was then determined up to 14,280 cycles.

[Fig. 9]

Figure 9 shows the friction coefficient plots for different albumin concentrations of 0, 1 and 20 $g.L^{-1}$. Until 7400 cycles, friction coefficient values at 1 $g.L^{-1}$ remained higher than those at 0 $g.L^{-1}$.

Meanwhile, the friction coefficient values at 20 $g.L^{-1}$ were higher than those at 0 $g.L^{-1}$ in the secondary and tertiary stages. It was found that the addition of albumin increases the friction coefficient. Friction coefficient evolutions for 1 and 20 $g.L^{-1}$ can be analyzed with Equation 1. The beginning of the friction test is submitted to several mechanical and chemical phenomena (alignment of samples, steady-state composition of the solution between materials in contact, for example). Thus, at the threshold of 7400 cycles, the friction coefficient for an albumin content of 1 $g.L^{-1}$ becomes lower than that at 0 $g.L^{-1}$, but is not reproducible, as determined by multiple experiments. Thus, another approach is suggested: the evolution of the energy ratio vs. the number of cycles.

[Fig. 10]

Figure 10 shows the evolution of the energy ratio with cycle number for tests with and without albumin. All energy ratios remained above 0.2 during the entire fretting cycle. In particular, the energy ratio measured with 1 $g.L^{-1}$ of albumin was greater than 0.55. In addition, after 3,000 cycles, the ratio for 1 $g.L^{-1}$ was higher than those for 0 and 20 $g.L^{-1}$. At the beginning of the test, the energy ratios related to 0 and 1 $g.L^{-1}$ are close. One might suggest that 2 groups should be constituted: the first with 0 and 1 $g.L^{-1}$ and the second with 20 $g.L^{-1}$. From these results, which come from usual tests in fretting (and fretting corrosion), the energy ratio effectively describes the expected lubricant effects of albumin. At this ionic strength, i.e. 0.001 M, corrosion of 316L SS is weak. However it occurs in conjunction with mechanics, with mechanics and corrosion being synergistically related. Notwithstanding, the energy approach is globalized and, as mentioned, the separation of the energy ratio at 0 $g.L^{-1}$ of albumin from that at 1 $g.L^{-1}$ is difficult. This is the reason why the analysis related to the damage rate constant should be useful.

[Table 1]

[Fig. 11]

Table 1 shows the damage rate constant and the damage exponent for albumin contents of 1 and 20 $g.L^{-1}$. The damage exponent values are close to -1. Meanwhile, the damage rate constant tends to increase as the albumin content increases (Figure 11). One should consider that the damage rate constant at 0 and 1 $g.L^{-1}$ are of the same order of magnitude. In Figure 11, the concentration of NaCl is equal to 0.001 M and the mechanical degradation is dominant. More generally, at this low concentration of NaCl, during fretting corrosion tests, protein (i.e albumin) promotes the effect of mechanics on the corrosive wear, with the results coming from Ref. [7]. Otherwise, from Ref. [7], albumin protects the 316L SS against the corrosion during fretting corrosion degradation. Thus, the approach suggested by Relation (3), and especially the damage rate constant, is useful for describing wear when the effect of corrosion can be neglected in an aqueous environment; the damage rate constant increases according the albumin content.

In summarizing the results in Figures 9, 10 and 11, the friction coefficient is difficult to interpret with respect to the albumin content, that the energy ratio vs. number of cycles describes well the expected lubricant effect of proteins, and that the evolution of the damage rate constant highlights that the effect of mechanical degradation is promoted when the albumin concentration increases, as expected [7]. Additional investigations should be carried out to explore this interesting relationship.

3.4 Influence of pH

[Fig. 12]

In order to investigate the influence of pH, two fretting corrosion tests were conducted in solutions with pH = 4 and pH = 7, as shown in Figure 12. Other conditions were an ionic strength of 1 M, zero albumin content, and open circuit conditions. The friction coefficient vs cycle number plots comprise three different stages, similar to those displayed in Figure 2. The initial friction coefficient at pH = 4 was about 0.55 and subsequently dropped to 0.43. Then, the friction coefficient increased with respect to the number of cycles. The difference between the maximum and the minimum values in the friction coefficient is quite significant. That is, an acidic solution degrades the contact surfaces, leading to the increase of friction during the fretting cycle.

[Fig. 13]

Figure 13 shows the evolution of the energy ratio with cycle number at different pH values. It was identified from the plot that all tests were conducted within the wear-dominant regime. After 5,000 cycles, the energy ratio for pH = 4 remained 0.52, but that for pH = 7 it was 0.44. At the "free pH", i.e. the pH of an unbuffered solution (but containing atmospheric CO_2 to give a pH of about 6.3), the energy ratio was the highest. It could be suggested that wear degradation dominates at the free pH, in comparison with buffered solutions (pH = 4 and pH = 7). At the free pH in the entire solution, one might suggest that the local pH, in the wear track area, could reach a low value due to crevice action and metal cation hydrolysis [20]. Thus, the wear track area is preferentially destroyed (to create rough surfaces) and more energy is necessary to affect the relative motion between surfaces in contact. *De facto*, one might suggest that free pH involves the highest degradation during fretting corrosion of the contact constituted by PMMA and 316L SS. The crevice effect, inside the wear track area of 316L SS, is one of the principal factors for explaining the highest wear at the free pH and consequently the highest dissipated energy (showed by energy ratio) during experimental tests. In the presence of a buffer, the lowering of the pH in the wear track is expected to be considerably muted.

[Table 2]

[Fig. 14]

Table 2 shows curve fitting result of the friction coefficient versus cycle number obtained at pH = 4 and pH = 7. The results show that the damage exponent is close to -1 and that the damage rate constant was variable. The damage rate constant of pH = 4 was two times greater than that at the free pH. In addition, the value at pH = 4 was greater than that at pH = 7 as shown in Figure 14. The free pH does not promote exhaustive mechanical wear, as highlighted by the evolution of the damage rate constant. This free pH is associated with the lowest damage rate constant. Thus the wear of 316L SS should be more promoted by the synergistic effect of mechanics on corrosion as expected [21]. It was suggested that pH decreases due to ohmic drop (similar to a crevice effect), and acidification finally occurs due to fretting. Thus, locally, pure mechanical degradation should be weak compared with that related to corrosion and accelerated corrosion, due to the crevice effect in the fretting zone. The principle of crevice acidification is described in Ref. [20]. Unfortunately, the mechanism of fretting corrosion is not uniform on the surface of 316L SS, with the micrographs in Reference [21] highlighting these heterogeneities. However, locally, as with classical pitting and crevice corrosion, the mechanism of acidification and the 'W' wear track should occur, as described

in Reference [20].

4. Conclusions

This paper investigated the friction behaviour under cyclical loading of 316L SS on PPMA in solutions of various ionic strengths, albumin concentration, and pH values. Fretting corrosion tests were conducted using a cylinder-to-plane contact configuration. Stainless steel and PMMA were used for femoral stem and bone cement, simulated contact for hip prosthesis. Measured evolutions of the friction coefficient were analyzed and the following conclusions were drawn.

- The evolution of the friction coefficient can be divided into three stages. In the primary (first) stage, the friction coefficient decreases, although this stage did not appear at some ionic strength values. In the secondary stage, the friction coefficient growth rate can be expressed with a power-law function of cycle number. Two coefficients are extracted from this law: the damage rate constant and the damage exponent. In the tertiary stage, the friction coefficient remained steady or displayed only a small decrease.
  - The damage rate constant can be used for quantifying the influence of ionic strength, albumin concentration, and pH on the evolution of the friction coefficient Ionic strength: the damage rate constant values for ionic strengths between 0.001 and 0.1 M were similar. Meanwhile, when the ionic strength was greater than 0.1 M, the damage rate constant significantly decreased as the ionic strength increased, due to enhancement of 316L synergistic corrosion.
  - Addition of albumin: the damage rate constant increased with increasing albumin content. The effect of mechanics on the corrosion is promoted, especially for the highest ionic strength.
- The friction coefficient at -0.4 V/SCE was higher than that at the open circuit potential (OCP) between -0.4V/SCE and -0.5 V/SCE.. An inverse linear relation was obtained between the friction coefficient and the measured potential.
- The evolution of the energy ratio and the damage rate constant, depended upon the pH. The free pH, around 6.3, probably promotes chemical degradation assisted by mechanics by the lowering of the unbuffered pH in the wear track.

Acknowledgements

This work was supported by a 2012 Korea Aerospace University Faculty Research Grant and by Agence Nationale de la Recherche (France) on the ‘Opt-Hip’ ‘ANR’ project. In addition, the authors wish to acknowledge the Region Rhône-Alpes for granting the stay at Penn State University.

Appendix A: Curve fitting

Power law form: $f=a*N^b$			
Ionic strength ($mol.L^{-1}$)	**A**	**b**	**R**
0.001	1.0164	0.0541	0.9978
0.010	1.0479	0.0537	0.9882
0.100	1.1484	0.0425	0.9834
0.155	1.2767	0.0256	0.9988
1.000	1.3512	0.0176	0.9859

Appendix B: Transition between the primary and secondary stages

Ionic strength ($mol.L^{-1}$)	**Number of cycles in the beginning of the secondary stage**
0.001	241
0.010	363
0.100	241
0.155	1
1.000	1

Albumin ($g.L^{-1}$)	**Number of cycles in the beginning of the secondary stage**
0	1
1	481
20	722

pH	**Number of cycles in the beginning of the secondary stage**
7	363
4	241
Free	122

References

[1] Waterhouse RB. Occurrence of fretting in practice and its simulation in the laboratory, materials evaluation under fretting conditions, in: ASTM STP 780, S.R. Brown; 1982, p. 3-16.

[2] Langlais F. Prothèses totales de hanche. Facteurs biologiques et mécanismes de tolérance, in: F. Langlais, J.P. Delagoutte (Eds.), Cahiers d'enseignement de la SOFCOT n◦44, Expansion scientifique française; 1993, p. 3–22.

[3] Ren W, Yang S, Fang H, Hsu S, Wooley PH. Distinct gene expression of receptor activator of nuclear factor-kB and rank ligandin the inflammatory response to variant morphologies of UHMWPE particles, Biomaterials 2003;24:4819–4826.

[4] Affatato S, Fernandes B, Tucci A, Esposito L, Toni A. Isolation and morphological characterisation of UHMWPE wear debris generated in vitro, Biomaterials 2001;22:2325-2331

[5] Gelb H, Schumacher HR, Cuckler J, Ducheyne P, Baker DG. In vivo inflammatory response to polymethylmethacrylate particulate debris: effect of size, morphology, and surface area, J Orthop Res 1994;12:83–92

[6] Hallab NJ, Jacobs JJ. Implant Debris: Clinical Data and Relevance, Comprehensive Biomaterials 2011;6:97-107

[7] Kovacs P, Davidson JA, Daigle K. Correlation between the metal ion concentration and the fretting wear volume of orthopaedic implant metals, particulate debris from medical implants: mechanisms of formation and biological consequences, in: ASTM STP 1144, ASTM International; 1997, p. 160-176.

[8] Tritschler B, Forest B, Rieu J. Fretting corrosion of materials for orthopaedic implants: a study of a metal/polymer contact in an artificial physiological medium, Tribol Int 1999;32:587-596.

[9] Geringer J, Forest B, Combrade P. Fretting-corrosion of materials used as orthopaedic implants, Wear 2005;259:943-51.

[10] Rubin PJ, Leyvraz PF, Rakotomanana LR. Intérêt de la modélisation numérique dans l'évaluation pré-clinique d'une prothèse fémorale de la hanche, Maîtrise Orthopédique 2000;93:22-27.

[11] Pellier J, Geringer J, Forest B. Fretting-corrosion between 316L SS and PMMA: Influence of ionic strength, protein and electrochemical conditions on material wear. Application to orthopaedic implants, Wear 2011;271:1563-71.

[12] Korsunsky AM, Kim K. Dissipated energy and friction coefficient evolution during fretting wear of solid lubricant coatings, Tribol Int 2010;43(5):861-7.

[13] Kim K, Korsunsky AM. Dissipated energy and fretting damage in CoCrAlY-MoS_2 coatings, Tribol Int 2010;43(3):676-84.

[14] Fouvry S, Kapsa P, Zahouani H, Vincent L. Analysis in fretting of hard coatings through a dissipated energy concept, Wear 1997;203:393-403.

[15] Katta JK, Marcolongo M, Lowman A, Mansmann KA. Friction and wear behaviour of ploy(vinyl alcohol)/poly(vinyl pyrrolidone) hydrogels for articular cartilage replacement, J Biomed Mater Res 2007;83(2):471-9.

[16] Gispert MP, Serro AP, Colaco R, Saramago B, Friction and wear mechanisms in hip prosthesis: Comparison of joint materials behaviour in several lubricants, Wear 2006;260:149-58.

[17] Nuño N, Amabili M, Groppetti R, Rossi A. Static coefficient of friction between Ti-6Al-4V and PMMA for cemented hip and knee implants, J Biomed Mater Res 2002;59(1):191-200.18] Nuño N, Groppetti R, Senin N. Static coefficient of friction between stainless steel and PMMA used in cemented hip and knee implants, Clin Biomech 2006;21:956-62.

[19] Geringer J, Forest B, Combrade P. Wear of Poly (methyl methacrylate) against a metallic surface in dry conditions, Polymer Eng Sci 2007;47(5)633-48.
[20] Geringer J, Macdonald D.D. Modeling fretting-corrosion wear of 316L SS against poly(methyl methacrylate) with the Point Defect Model: Fundamental theory, assessment, and outlook, Electrochim. Acta 2012;79:17-30
[21] Geringer J, Pellier J, Taylor ML, Macdonald DD. Fretting corrosion with proteins: the role of organic coating on the synergistic mechanisms, Surf Coat Tech 2012 accepted, in press

Figures

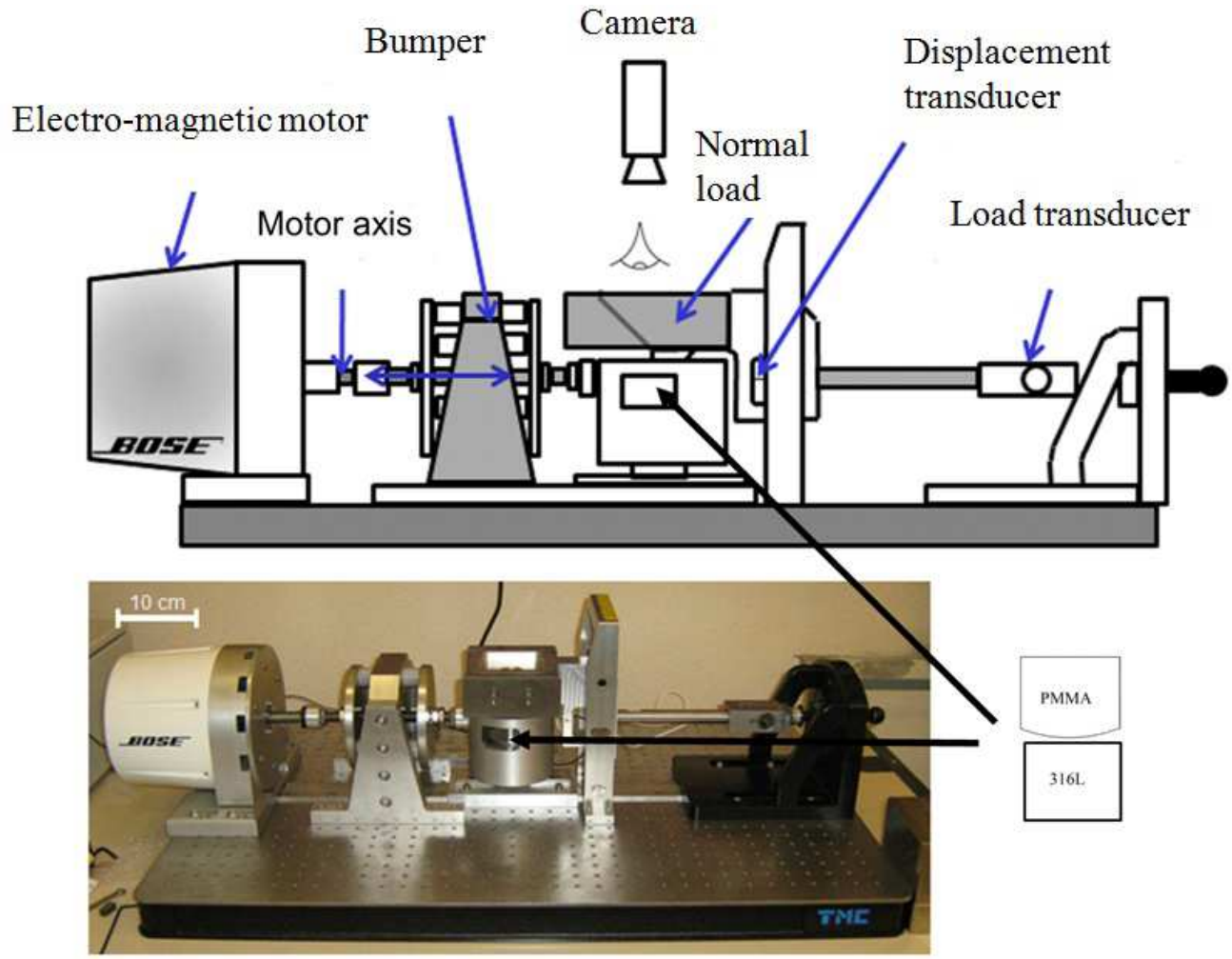

Fig. 1. Fretting corrosion testing machine [7].

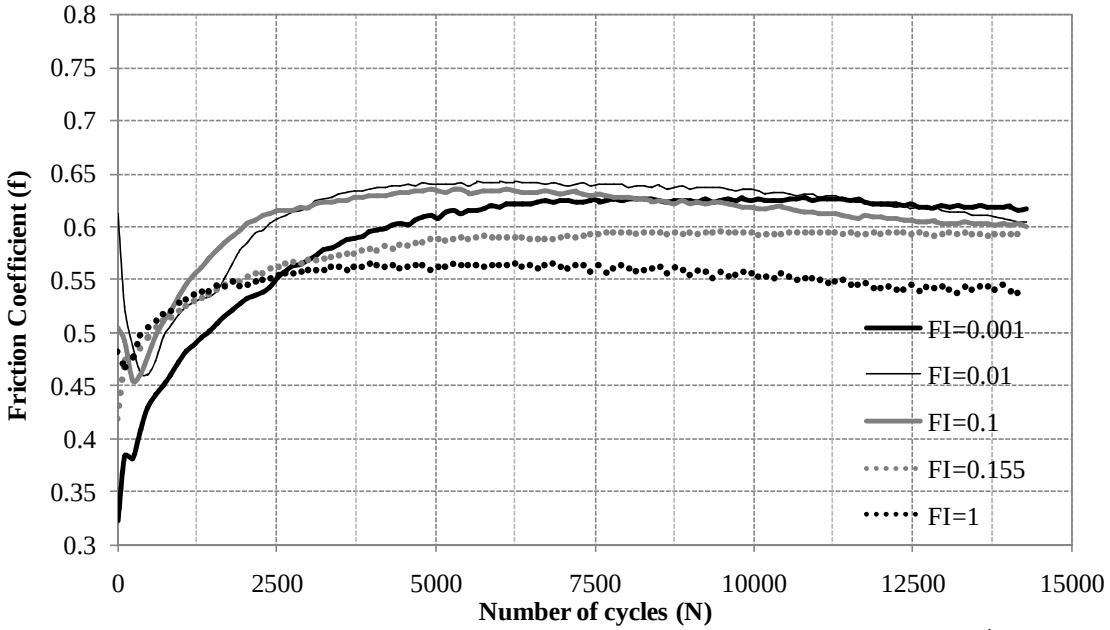

Fig. 2. Friction coefficient evolutions at various ionic strengths, FI ($mol.L^{-1}$). Tests were conducted at OCP and without albumin.

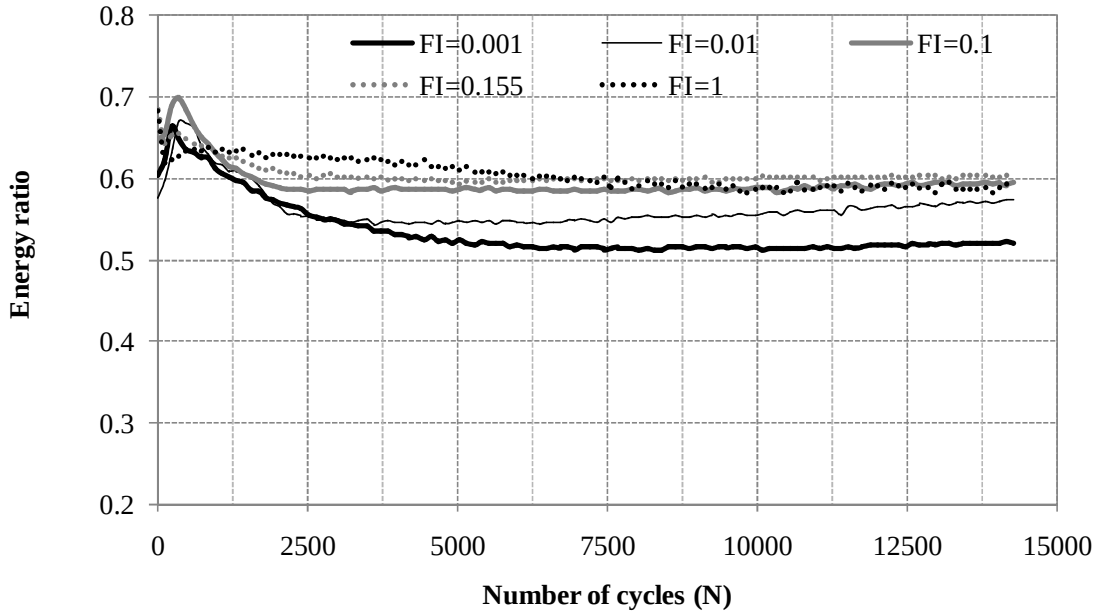

Fig. 3. Evolution of energy ratio at various ionic strengths, FI ($mol.L^{-1}$). Tests were conducted at OCP and without albumin.

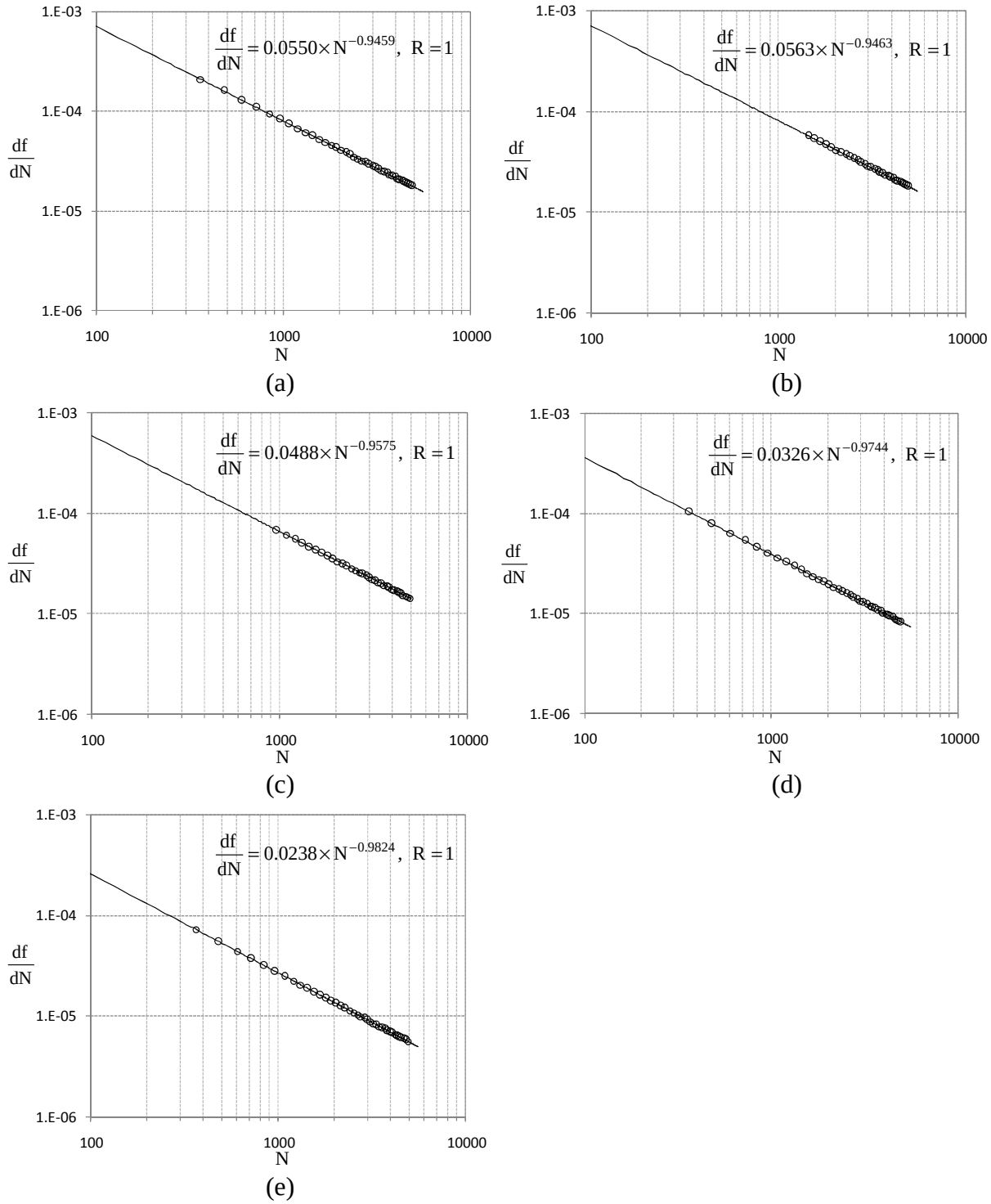

Fig. 4. *df/dN* versus N plots on the bilogarithmic scale for the determination of parameters C and *m*. The points came from the curve fit. (a) 0.001 mol.L^{-1}, (b) 0.01 mol.L^{-1}, (c) 0.1 mol.L^{-1}, (c) 0.155 mol.L^{-1} and (d) 1 mol.L^{-1}. Tests were conducted without albumin and at OCP.

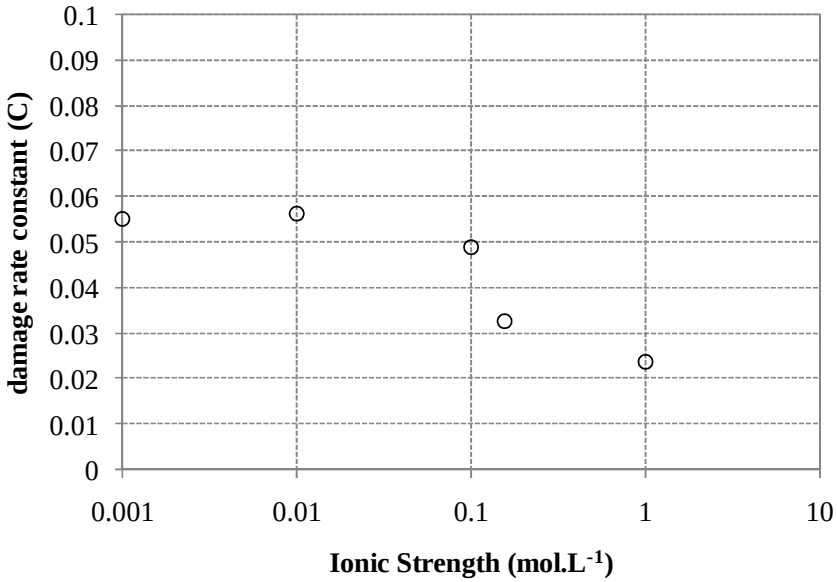

Fig. 5. Relation between the damage rate constant and ionic strength. Tests were conducted without albumin and at OCP.

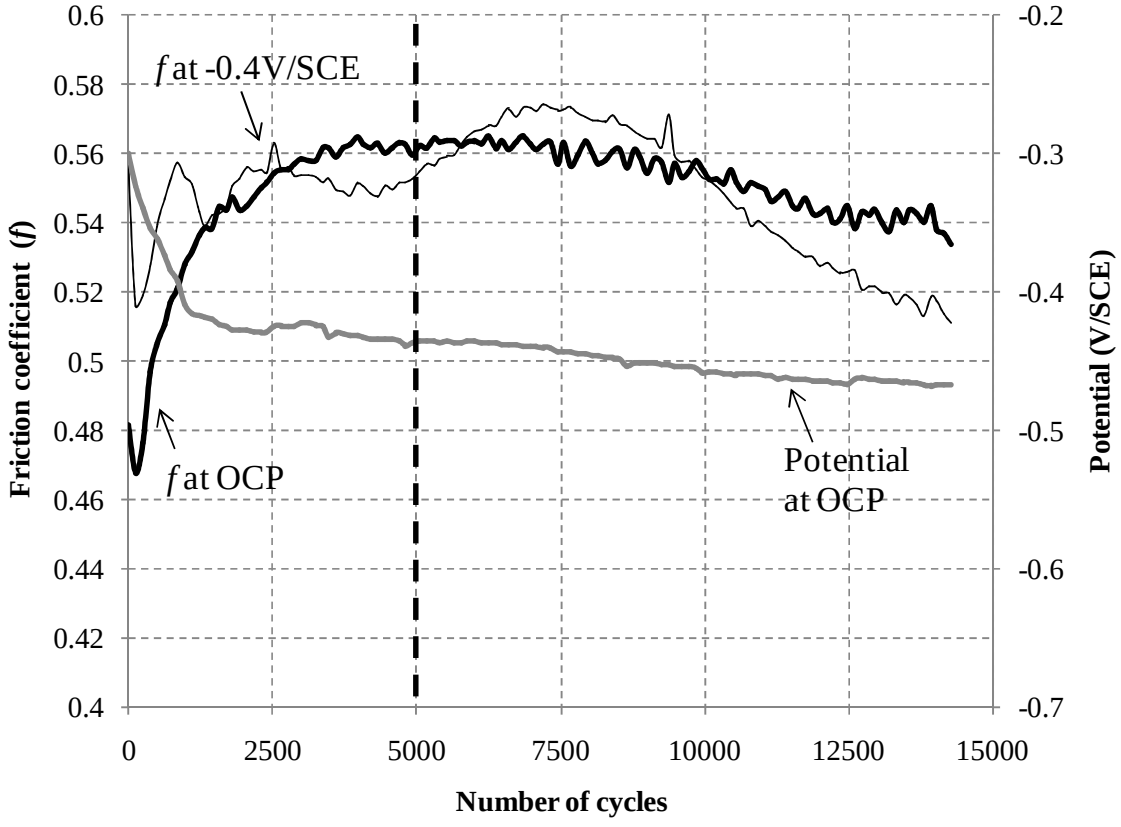

Fig. 6. Difference of friction coefficient evolutions between OCP and -0.4 V/SCE. The potential indicates the value for the test performed at OCP. Tests were conducted at 1 mol.L^{-1} of ionic strength and at albumin of 0 g.L^{-1}.

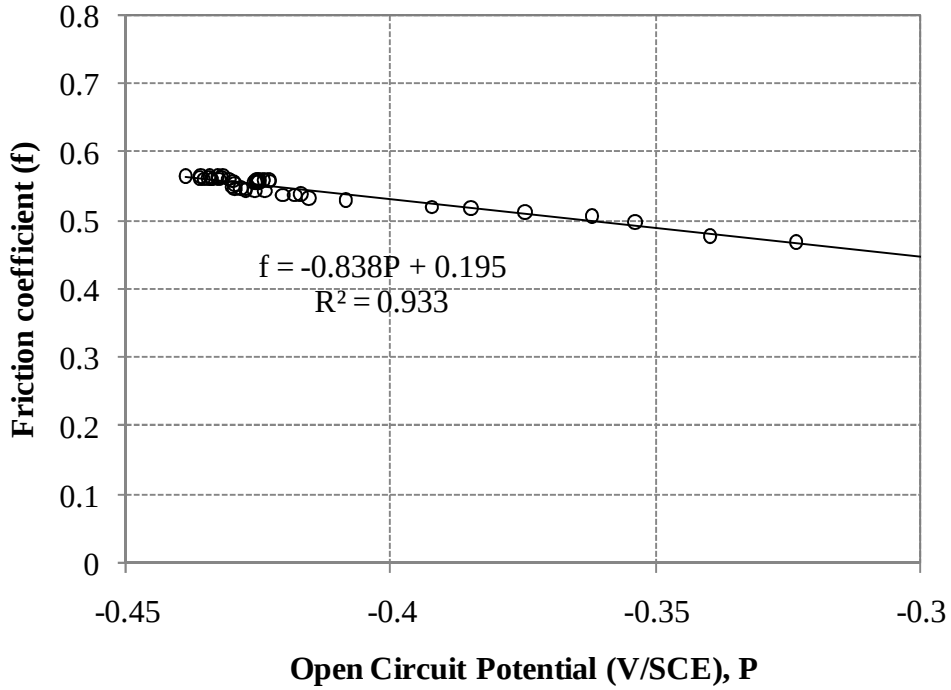

Fig. 7. Relation between friction coefficient and Open Circuit Potential within 5000 cycles. Tests were conducted at ionic strength of 1 mol.$L^{-1}$and at albumin of 0 g.L^{-1}.

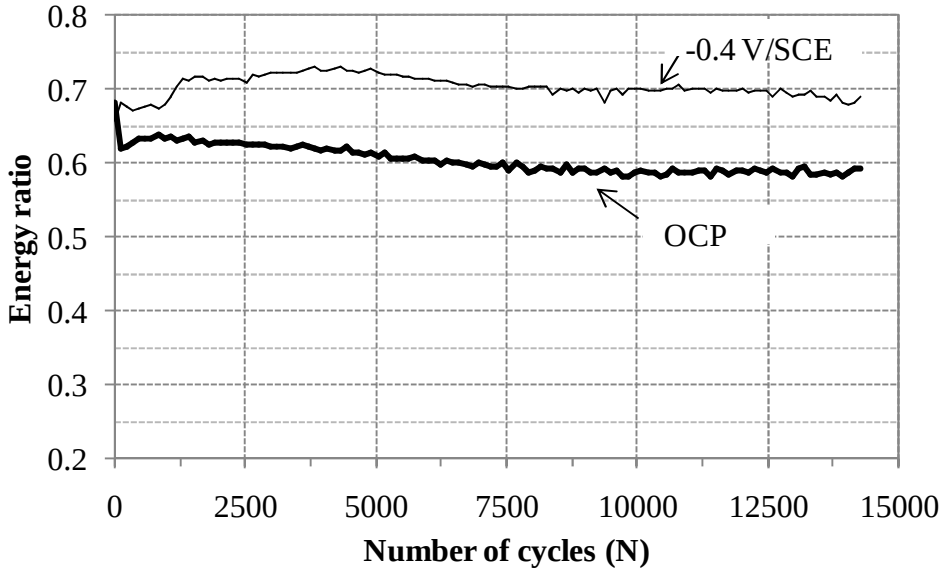

Fig. 8. Evolution of energy ratio at OCP and -0.4 V/SCE. Tests were conducted at ionic strength of 1 mol.$L^{-1}$and at albumin of 0 g.L^{-1}.

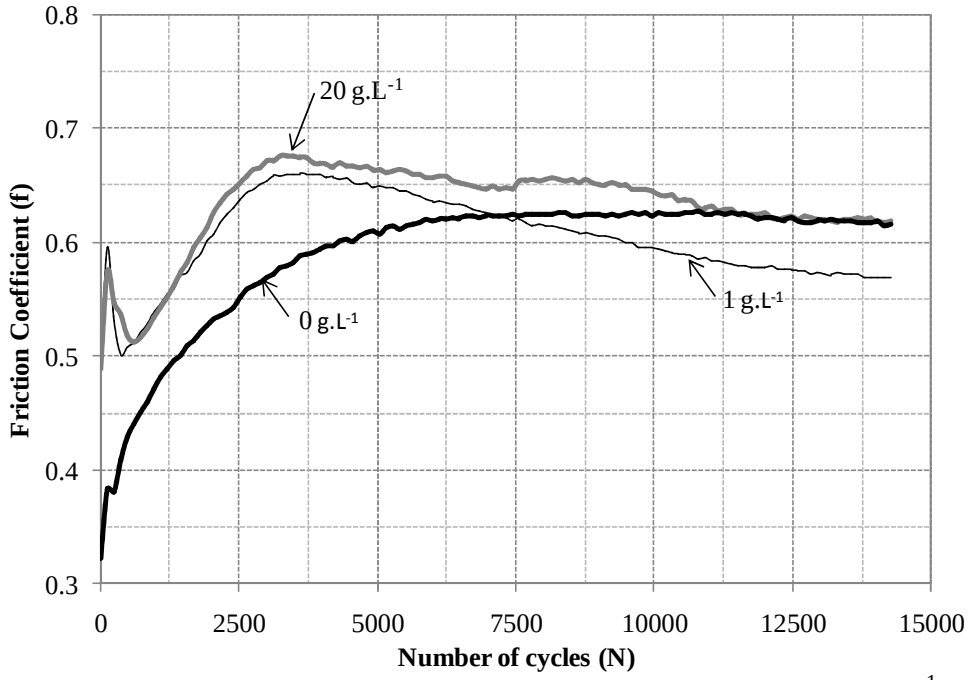

Fig. 9. Friction coefficient evolutions according to albumin content ($g.L^{-1}$), respectively. Tests were conducted at ionic strength of 0.001 $mol.L^{-1}$ and at OCP.

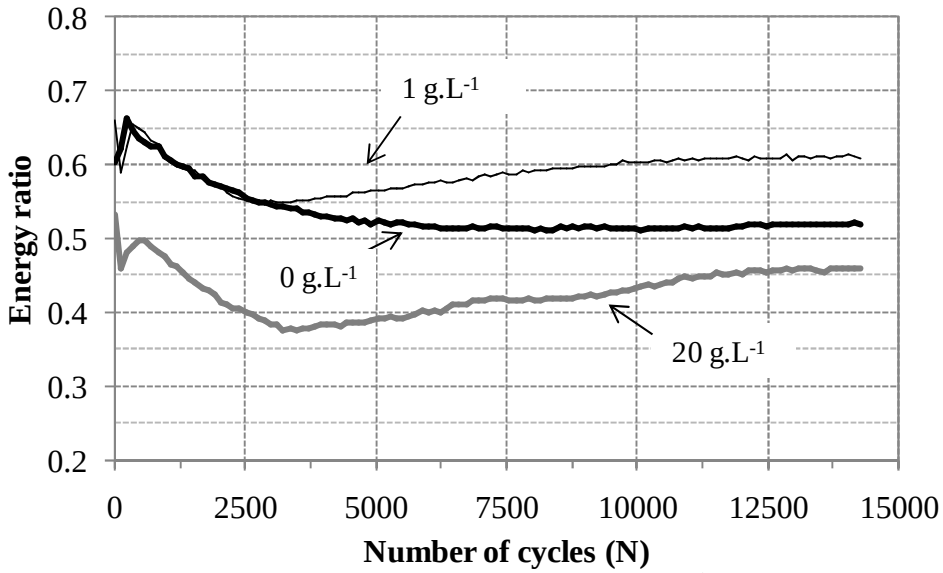

Fig. 10. Evolution of energy ratio at different albumin content ($g.L^{-1}$). Tests were conducted at ionic strength of 0.001 $mol.L^{-1}$and at OCP.

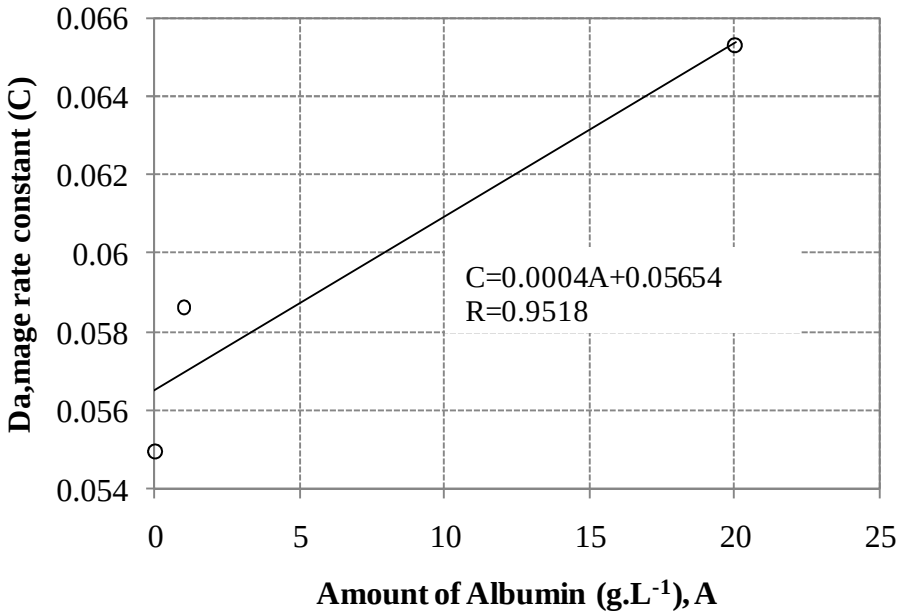

Fig. 11. Relation between the damage rate constant and the albumin content. Tests were conducted at 0.001 mol.L^{-1} of ionic strength and at OCP.

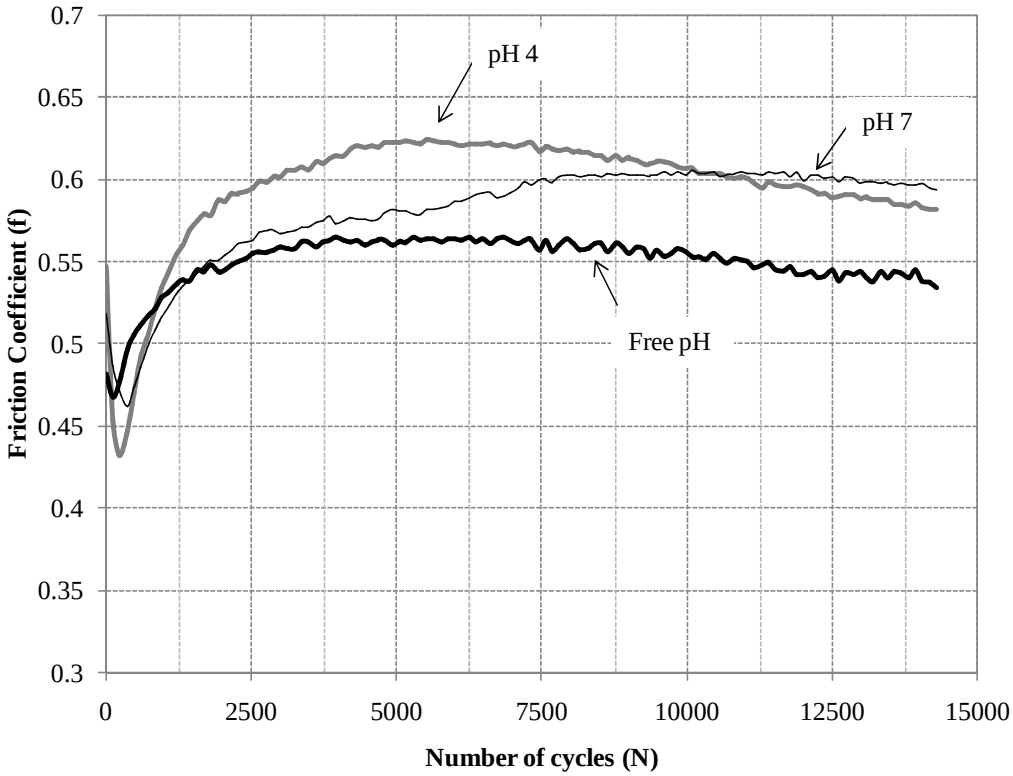

Fig. 12. Friction coefficient evolution at different pH conditions. Conditions: ionic strength of 1 mol.L^{-1}, zero albumin, and OCP.

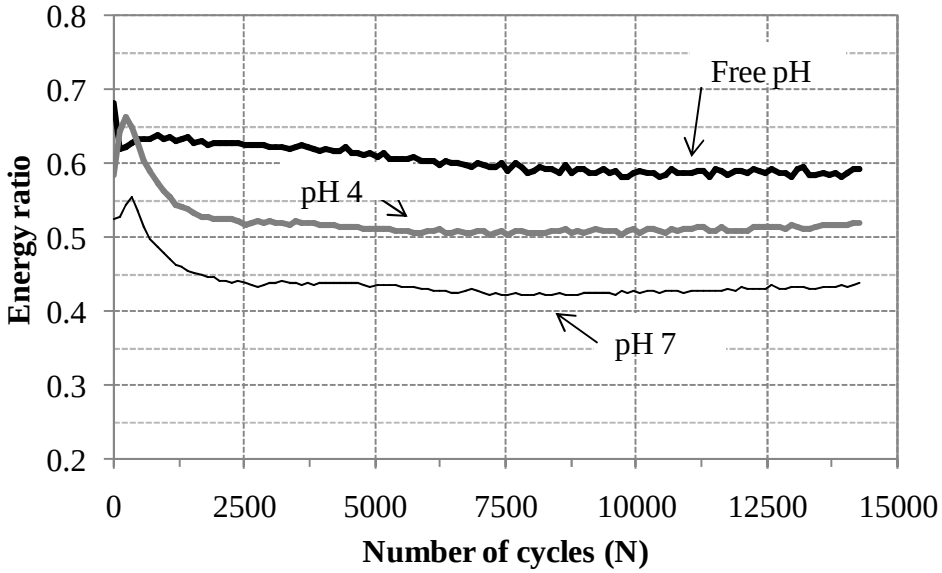

Fig. 13. Evolution of energy ratio at different pH. Conditions: ionic strength of 1 mol.L^{-1}, zero albumin, and OCP.

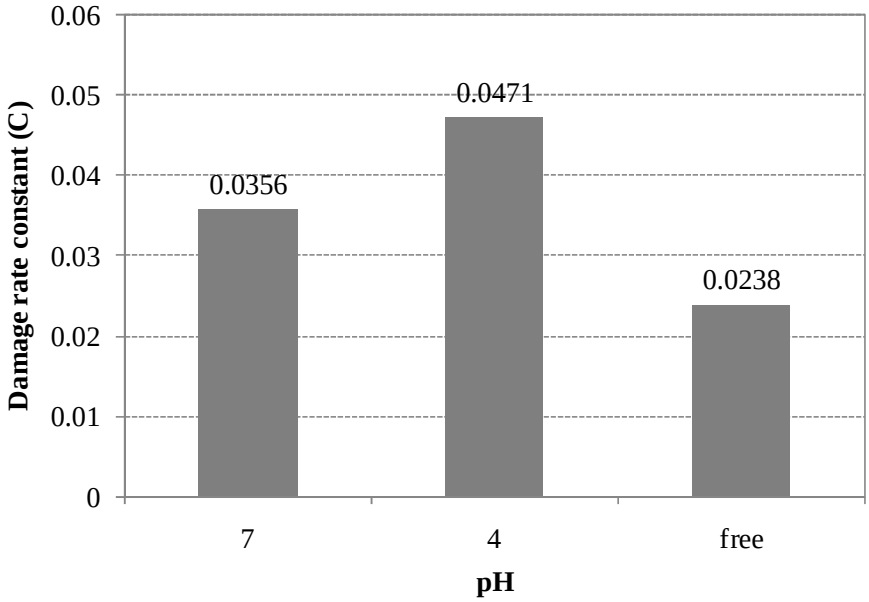

Fig. 14. Damage rate constant versus pH plot. Conditions: ionic strength of 1 mol.L^{-1}, zero albumin, and OCP.

Tables

Table 1. Parameters C and m at different albumin content ($g.L^{-1}$).

Albumin ($g.L^{-1}$)	**Damage rate constant (C)**	**Damage exponent (m)**	**R**
0	0.0550	-0.946	0.99
1	0.0586	-0.944	0.99
20	0.0653	-0.933	0.99

Table 2. Parameters C and m at different pH.

pH	**Damage rate constant (C)**	**Damage exponent (m)**	**R**
7	0.0357	-0.971	0.99
4	0.0471	-0.959	0.99
Free	0.0238	-0.982	0.99